Measurements of in-plane thermophysical properties on nanoscale-thick films by lock-in thermography

Abdulkareem Alasli,[1,*] Ryo Iguchi,[2] Ken-ichi Uchida[2,3], and Hosei Nagano[1]

[1] Department of Mechanical Systems Engineering, Nagoya University, Nagoya 464-8601, Japan
[2] National Institute for Materials Science, Tsukuba 305-0047, Japan
[3] Department of Advanced Materials Science, Graduate School of Frontier Sciences, The University of Tokyo, Kashiwa 277-8561, Japan
[*] Authors to whom correspondence should be addressed: al.asli.abdulkareem.m6@f.mail.nagoya-u.ac.jp

Abstract

We demonstrate a versatile technique for measuring the in-plane thermal conductivity, in-plane thermal diffusivity, and volumetric heat capacity of nanoscale-thick films by means of lock-in thermography. The technique relies on the thermal analyses of the imaged lock-in temperature distribution over the surface of the films generated by an on-chip line heater. This enables simultaneous estimation of the properties for a free-standing membrane or multilayered thin films deposited on the membrane. We validate the usability of the technique by determining the thermophysical properties of Ni films with different nanoscale thicknesses. This technique also enables the measurements under an external magnetic field, facilitating investigating magneto-thermal transport properties. Thus, the proposed approach will be useful for exploring nanoscale thermal transport properties in thin films and thermal management systems.

Thin films refer to a class of materials of small thicknesses ranging from sub-nanometers to a few micrometers. Due to their unique properties, thin films are widely implemented in various applications including electronics,[1] microelectromechanical systems,[2,3] thermal barrier coatings,[4] optoelectronics,[5] spintronics,[6] magnetics,[7] and thermoelectrics.[8] Characterizing thermophysical properties and understanding thermal behaviors of thin films are crucial for optimizing the performance and stability of these applications. They also play a key-role in elucidating the physical phenomena behind the store, conversion, and transport of thermal energy in such thin structures, thereby pushing the limits for developing more advanced materials and systems with enhanced heat transfer and energy efficiency.

The thermophysical properties of thin films often exhibit distinct values and behaviors from their bulk counterparts.[9–11] This fact and the small physical dimension of the material made the accurate assessing of the properties quite challenging with conventional measurement techniques.[10] For instance, the thermal conductivity κ of thin films is often anisotropic, i.e., in-plane κ and out-of-plane κ conduct heat differently even for materials whose bulk form is isotropic. In-plane κ and out-of-plane κ may depend on the nanoscale thickness of the thin films and usually demonstrate lower values than of the bulk materials.[10,12] To accurately determine κ under these constraints, various methods, such as laser- and electrothermal-based techniques, have been intensively developed.[13] Among them, the 3ω method[14] and transient thermoreflectance technique in both time[15] and frequency[16] domains took the lead. Despite the outstanding performance of these methods for out-of-plane κ measurements, achieving the similar sensitivity and accuracy for in-plane κ measurements remains a challenge.[17,18] Determining additional thermophysical properties, such as in-plane thermal diffusivity D and volumetric heat capacity ρc_p, also entails analogous difficulties, where a wide range of complex and time-consuming experiments[19] with larger uncertainties are involved. This motivates the development of different approaches for measuring in-plane thermophysical properties of thin films.

A versatile approach for measuring multiple in-plane thermophysical properties of thin films can be achieved by means of lock-in thermography (LIT). LIT is an active thermal imaging technique that enables noncontact detection of the thermal response in a material to a periodic heating with high temperature resolution.[20] LIT has distinguished itself in measuring various properties including D,[21] interfacial thermal resistance,[22] mapping thermophysical properties of composites,[23] thermoelectric figure of merit,[24,25] magneto-thermoelectric effects,[26–28] thermo-spin effects,[29,30] as well as magnetocaloric,[31] elastocaloric,[32] and electrocaloric effects.[33] Reference 34 has offered a LIT-based method for analyzing the in-plane thermophysical properties of a single free-standing thin film at micrometer-scale thickness with a line-shaped laser light as a heating source. Nevertheless, the measurements are impeded by the need to ascertain the optical properties of the film to quantify the coupled power from the laser, which is essential to determine in-plane κ and ρc_p.[34] The measurement accuracy is also noticeably affected by the width and uniformity of the laser line, and the need for double-side black paint coating (~15 μm on each side) to enhance the absorptivity and emissivity of thin films.[34] In this paper, we facilitate the LIT-based method to enable the determination of the in-plane D, in-plane κ, and ρc_p for nanoscale-thick single or multilayered films with high sensitivity and reliability. With the versatility of this technique, we extend the measurements under magnetic fields, enabling systematic investigations on magneto-thermal transport/resistance properties of thin films.

Figure 1 illustrates the main principle of the LIT-based measurement method. This method enables the determination of thermophysical properties in single-layer or multilayer thin film structures. The setup consists of an infrared camera connected to an LIT processing system and a current source. The sample can take the form of a single-layer or multilayer thin film structure, either free-standing or deposited on a suspended membrane. The heating source is a thin metallic line heater deposited on the other side of the structure with the configuration shown in Fig. 1. The line heater is excited by the current source with a half square-wave-modulated charge current with the frequency f, amplitude J_{c}, and DC offset $J_{\mathrm{c}}/2$. Subsequently, an oscillating heat release due to the Joule heating $Q = RJ_{\mathrm{c}}^2$ is induced in the line heater with the same f, where R is the resistance of the line heater. Q diffuses symmetrically within the membrane/thin film structure depending on their effective in-plane thermal diffusivity D_{eff}, effective in-plane thermal conductivity κ_{eff}, and effective volumetric heat capacity $(\rho c_{\mathrm{p}})_{\mathrm{eff}}$ defined as follows:[35]

$$D_{\mathrm{eff}} = \frac{\sum \kappa_n t_n}{\sum \frac{\kappa_n}{D_n} t_n}, \tag{1}$$

$$\kappa_{\mathrm{eff}} = \frac{\sum \kappa_n t_n}{\sum t_n}, \tag{2}$$

$$(\rho c_{\mathrm{p}})_{\mathrm{eff}} = \frac{\sum (\rho c_{\mathrm{p}})_n t_n}{\sum t_n}, \tag{3}$$

where t_n is the thickness of the layer n. The infrared camera images the transient temperature modulation $\tilde{T}$ response on the thin film side by taking the directional spectral emissivity of the thin film and detectable wavelength range of the camera sensor into consideration. The LIT system accordingly extracts the amplitude A and phase lag ϕ of $\tilde{T}$ at the first harmonic by the Fourier analysis at each pixel. The A and ϕ images show the spatial distribution of the magnitude and time delay of $\tilde{T}$ due to the heat diffusion, respectively. By performing the thermal analyses on the LIT images, we can obtain the in-plane D_{eff}, in-plane κ_{eff}, and $(\rho c_{\mathrm{p}})_{\mathrm{eff}}$ [Fig. 1 (b)], as detailed below.

To perform the thermal analyses, we solve the one-dimensional heat equation along the transverse axis x for an infinitely large thermally thin n-layer structure with the line heater located at $x = 0$ (Fig. 1).[34,36] By accounting for the heat loss effects of thermal radiation and convection through the combined heat transfer coefficient h,[12,34] A and ϕ of the steady periodic solution of $\tilde{T}$ at in relation to the first harmonic of Joule heating are respectively

$$A(x) = \left|\tilde{T}(x)\right| = \frac{RJ_\mathrm{c}^2}{\pi\kappa_\mathrm{eff} l t_\mathrm{tot}}\left(\sqrt{\left(\frac{\omega}{D_\mathrm{eff}}\right)^2 + \left(\frac{2h}{t_\mathrm{tot}\kappa_\mathrm{eff}}\right)^2}\right)^{-1/2} e^{-|x|/\Lambda_\mathrm{A}}, \tag{4}$$

$$\phi\,(x) = -\arg[\tilde{T}(x)] = +\frac{|x|}{\Lambda_\phi} + \tan^{-1}\frac{\Lambda_A}{\Lambda_\phi} - \frac{\pi}{4}, \tag{5}$$

where κ_eff is the effective thermal conductivity of the structure, l the heater length, $t_\mathrm{tot} = \sum t_n$ the sum of the layer thicknesses, and $\omega = 2\pi f$ the angular frequency. Λ_A and Λ_ϕ are respectively the thermal diffusion lengths of A and ϕ, which are expressed as

$$\Lambda_A = \left(\sqrt{\left(\frac{\omega}{2D_\mathrm{eff}}\right)^2 + \left(\frac{h}{t_\mathrm{tot}\kappa_\mathrm{eff}}\right)^2} + \frac{h}{t_\mathrm{tot}\kappa_\mathrm{eff}}\right)^{-1/2}, \tag{6}$$

$$\Lambda_\phi = \left(\sqrt{\left(\frac{\omega}{2D_\mathrm{eff}}\right)^2 + \left(\frac{h}{t_\mathrm{tot}\kappa_\mathrm{eff}}\right)^2} - \frac{h}{t_\mathrm{tot}\kappa_\mathrm{eff}}\right)^{-1/2}. \tag{7}$$

By utilizing Eqs. (4)-(7), in-plane D_eff, in-plane κ_eff, and $\left(\rho c_\mathrm{p}\right)_\mathrm{eff}$ are obtained as follow, as also summarized in Fig. 1(b). In-plane D_eff can be first obtained from the geometric mean

$$\sqrt{\Lambda_A\Lambda_\phi} = \sqrt{\frac{2D_\mathrm{eff}}{\omega}}, \tag{8}$$

by measuring Λ_A and Λ_ϕ at a specific ω.[37] On the other hand, in-plane κ_eff and h can be determined from the difference

$$\frac{1}{\Lambda_A^2} - \frac{1}{\Lambda_\phi^2} = \frac{2h}{t_\mathrm{tot}\kappa_\mathrm{eff}}, \tag{9}$$

and A [Eq. (4)] at the line heater position with the knowledge of t_tot, l, J_c, and R. It is important to emphasize here that a temperature calibration of the LIT system is required for this step to determine A quantitatively (Sec. S1 in the supplementary material). Finally, $\left(\rho c_\mathrm{p}\right)_\mathrm{eff}$ can be extracted from

$$\left(\rho c_\mathrm{p}\right)_\mathrm{eff} = \frac{\kappa_\mathrm{eff}}{D_\mathrm{eff}}. \tag{10}$$

Equations (4)-(10) can be used to directly determine the effective properties of multilayered or the properties of single thin film structures from a single LIT measurement. However, to obtain the individual properties of each layer n in the multilayered thin film structure, a sequence of LIT measurements and analyses must be performed on sequenced deposited layers with taking into account Eqs. (1)-(3). It is critical to point out that this solution is valid under the following conditions. First, the suspended multilayered film/membrane structures should be thermally thin, meaning that the temperature gradient in the out-of-plane direction is negligibly small. This can be satisfied when the total thickness of the multilayer is much smaller than Λ.

To demonstrate the proposed LIT-based method, we measured and analyzed the thermal response from Ni thin films at different thicknesses. The 50-, 100-, and 150-nm-thick Ni thin films were deposited on a commercially available 200-nm-thick SiN membrane from NTT-AT Corporation, Japan, by the magnetron sputtering method. Further details on the structural characterization of the thin films are provided in Sec. S2 of the supplementary materials. The Au line heater with four-pads configuration was fabricated on the other side of the membrane by the lift-off process at a width of 15 μm and a thickness of 50 nm. For the LIT measurements, the thin film/membrane structure is positioned in the focal plane of a science grade infrared camera (SC5600, FLIR Systems, USA) with 5× lens and spectral response range of 2.5-5.1 μm with the thin film side facing the lens. For measuring the thermophysical properties of only the SiN membrane, the imaged side was coated with ~80 nm ultrapure (99.9%) high emissivity graphite by vapor-deposition based carbon coater (CADE-4TE, Meiwafosis CO., Japan) since the SiN membrane is highly transparent in the wavelength range of the camera.[38] This was not needed for the other Ni/SiN samples owing to the finite emissivity of the Ni films. The measurements of all samples were performed while applying J_c with a half-square wave form at f = 20 Hz to the line heater at room temperature to minimize the effect of heat losses.[25] R was measured by the four-probe method and the amplitude of J_c was adjusted to sustain a relatively equivalent Q for all measured samples. The thermal analyses were performed on LIT images obtained from >2000 periods at the maximum camera frame rate (100 Hz) at the full frame size after recaching the thermal equilibration.

Figure 2(a) shows the calibrated A/Q and ϕ images at f = 20.0 Hz for the samples with different Ni thicknesses. Figure 2(b) shows the corresponding line profiles along the x direction. A is divided by Q to eliminate the electrical properties of the line heater effect on the thermal response. A clear temperature modulation signal induced by Q from the line heater can be observed with the thermal diffusion pattern over the surface of the membrane and thin film structures. The magnitude of A/Q is maximized at the position of the line heater (x = 0 mm). The A/Q (ϕ) values then exponentially decay (linearly change) with the distance from the heater with symmetrical distribution [Fig. 2(b)]. Furthermore, the magnitude of A/Q notably decreases with the increment of the Ni thickness. The exponential decay rate of A/Q and the slope of ϕ also decrease with the Ni thickness increment, indicating a higher in-plane D_{eff} for the thicker Ni films on the membrane. These behaviors are consistent with Eqs. (4)-(7) as also emphasized by the fitting lines in Fig. 2(b), highlighting the ability of the LIT method in detecting the variations in thermal response in thin films due to the nanoscale thickness change.

Consequently, the thermophysical properties of the SiN membrane were directly obtained by analyzing the corresponding LIT images in Fig. 2 at $T = 298$ K. The in-plane D of SiN was determined to be 1.43 mm^2·s^{-1} from $\sqrt{\Lambda_A \Lambda_\phi}$ [Eq. (8)] by fitting the averaged A and ϕ data [Fig. 2 (b)] using Eqs. (3) and (4), respectively. Λ_A was extracted from the exponential decay rate of A, while Λ_ϕ is extracted from the slope of ϕ. Here, there is no direct effect from the A calibration or heat losses since $\sqrt{\Lambda_A \Lambda_\phi}$ depends only on in-plane D and ω [Eq. (8)]. Subsequently, the in-plane κ and h were obtained as 2.78 W·m^{-1}·K^{-1} and 4.74 W·m^{-2}·K^{-1}, respectively, from $1/\Lambda_A^2 - 1/\Lambda_\phi^2$ and A at the line heater ($x = 0$) [see Eq. (3)], involving two unknowns with two equations. Accordingly, ρc_p is 1.95 MJ·m^{-3}·K^{-1}. The obtained values here are consistent with the literature results for SiN membranes of similar thickness[39,40] However, it is important to emphasize that the accuracy of the A calibration (Secs. S1 and S3) play a key role in the accurate assessment of the in-plane κ and ρc_p. Moreover, the unavoidable usage of the black coating layer for the SiN membrane also affects the accuracy of the measurements. However, this effect can be compensated with the knowledge of the thickness and the thermophysical properties of the coating layer.[12,37]

With considering the thermophysical properties of SiN, the thickness dependence of the in-plane D, in-plane κ, and ρc_p at $T = 298$ K was obtained for the deposited Ni thin films, as plotted in Figs. 3(a)-3(c), respectively. The in-plane D, in-plane κ, and ρc_p for the Ni thin films exhibit obvious thickness dependence. The values of the in-plane D and in-plane κ (ρc_p) for the Ni films increase (decrease) with the thickness and approach the value of bulk Ni at a thickness of 150 nm. These behaviors are consistent with the previous observation on metal nanocrystalline materials.[41–45] The main reasons behind these behaviors can be attributed to the notable sputtered grain-boundary,[46] impurities, softening of surface phonons,[43] and defects in the nanocrystalline structure. The surface scattering of electrons also contributes to the reduction of the in-plane κ (and consequently the in-plane D) with decreasing thickness, given the considerable role of electronic part of κ in thin metallic films.[47–49] This also coincides with the observations that the electrical conductivity diminishes as the thickness of thin films decreases.[50,51] These effects decrease with the thickness increment and thus the properties approach the values of the bulk materials. The reported in-plane κ values of 83-nm-thick[50] and ~400-nm-thick[46] Ni thin films are respectively ~25 and ~65 $\mathrm{W\cdot m^{-1}\cdot K^{-1}}$, which are consistent with our measurements. These results show the capability of the LIT-based method in measuring the nanoscale thickness dependency of the in-plane thermophysical properties for thin films. It is important to emphasize here that achieving accurate and reliable measurements necessitates addressing potential sources of systematic error, implementing strategies to minimize them, and accounting for the sensitivity limitations inherent to the method, as detailed in Sec. S3 of the supplementary material.

To showcase the versatility of the method, we conducted the same LIT measurements and thermal analyses on the samples while applying a magnetic field **H**. A uniform **H** with the magnitude $\mu_0 H$ = 150 mT, with μ_0 being the vacuum permeability, was applied using an electromagnet. The potential sources of systematic errors (Sec. S3 in the supplementary material) were carefully considered in both parallel $\mathbf{H}_{\parallel}$ and perpendicular $\mathbf{H}_{\perp}$ orientations to the axis of the in-plane thermal gradient ∇T induced by the line heater (Fig. 1). We focused here on the field orientation dependence of the in-plane κ for the Ni film as a direct indicator of the magneto-thermal resistance effect since ρc_{p} is typically field independent.[24] Figure 4 shows the thickness dependence of in-plane κ for various magnetic field configurations (see also Sec. S4 in the supplementary material showing the corresponding LIT images). The results show good consistency with the values estimated from the LIT measurements performed with the absence of **H**. A small but finite decay in the in-plane κ was observed in the 100- and 150-nm-thick Ni films at the $\mathbf{H}_{\parallel}$ and $\mathbf{H}_{\perp}$ measurements, while no clear **H** dependence was observed for the 50-nm-thick film. Moreover, no obvious anisotropic magneto-thermal resistance behavior can be claimed for all the films. This result can be attributed to the low magneto-thermal resistance of Ni at room temperature,[52,53] which falls below the sensitivity of the used LIT system with respect to the low directional spectral emissivity of the metal thin films. Here we emphasize that all measurement and analysis procedures can be performed without any restrictions in the presence of magnetic fields. Thus, despite the absence of clear directional magnetic-field- or magnetization-dependent effects in the studied Ni thin films, the LIT-based method remains valuable as it allows for versatile measurements of the giant magneto-thermal resistance and **H** dependence of the thermophysical properties in spintronic multilayers. Importantly, although the current-perpendicular-to-plane giant magneto-thermal resistance in spintronic multilayers has been observed using the time-domain thermoreflectance method,[54,55] our LIT-based method enables the investigation of the current-in-plane giant magneto-thermal resistance, accelerating studies on spintronic thermal management.[56]

In conclusion, we presented a method for determining the in-plane thermophysical properties of nanoscale-thick films by means of the LIT technique. The in-plane D, in-plane κ, and ρc_{p} of a single or multilayered free-standing structure can be extracted from the thermal analyses of the transient temperature distribution induced by Joule heating from a deposited metallic line heater. This enables systematic and versatile investigations of thermophysical properties with high sensitivity and reliability. The validity and sensitivity of the method were demonstrated by measuring the thermal properties of the Ni thin films deposited on the suspended SiN membranes at different Ni thicknesses. The method also facilitates performing measurements under magnetic fields enabling the study of thermal magneto-resistance effects. Thus, the proposed LIT-based approach will be useful for the investigation of magneto-thermal transport/resistance, and thermoelectric properties, as well as thermal rectification effects in thin films.[57] To expand the scope of the method, future studies should incorporate direct electrical resistivity measurements of thin films, which requires redesigning the thin film structure to integrate a four-probe configuration. This enables more rigorous analysis of thermal and electrical transport properties.[50]

Supplementary material

See the supplementary material for details on the calibration of LIT detected temperature, structural characterization of the thin films, systematic sources of errors, and magnetic field dependence of temperature modulation signals.

Acknowledgments

This work was supported by CREST “Creation of Innovative Core Technologies for Nano-enabled Thermal Management” (Grant No. JPMJCR17I1) and ERATO "Magnetic Thermal Management Materials" (Grant No. JPMJER2201) from JST, Japan.

Disclosure statement

No conflict of interest was reported by the authors.

Data availability statement

The data that support the findings of this study are available from the corresponding author upon reasonable request.

References

[1] S. Gupta, W. Navaraj, L. Lorenzelli, and R. Dahiya, Npj Flex. Electron. **2**, 8 (2018).

[2] G. Sim, J. Krogstad, K. Reddy, K. Xie, G. Valentino, T. Weihs, and K. Hemker, Sci. Adv. **3**, e1700685 (2017).

[3] S. Takamatsu, S. Goto, M. Yamamoto, T. Yamashita, T. Kobayashi, and T. Itoh, Sci. Rep. **9**, 1893 (2019).

[4] N. Padture, M. Gell, and E. Jordan, Science **296**, 280 (2002).

[5] J. An, X. Zhao, Y. Zhang, M. Liu, J. Yuan, X. Sun, Z. Zhang, B. Wang, S. Li, and D. Li, Adv. Funct. Mater. **32**, 1 (2022).

[6] A. Hirohata, K. Yamada, Y. Nakatani, I. Prejbeanu, B. Diény, P. Pirro, and B. Hillebrands, J. Magn. Magn. Mater. **509**, 166711 (2020).

[7] X. Jiang, Q. Liu, J. Xing, N. Liu, Y. Guo, Z. Liu, and J. Zhao, Appl. Phys. Rev. **8**, 031305 (2021).

[8] I. Chowdhury, R. Prasher, K. Lofgreen, G. Chrysler, S. Narasimhan, R. Mahajan, D. Koester, R. Alley, and R. Venkatasubramanian, Nat. Nanotechnol. **4**, 235 (2009).

[9] A. Majumdar, J. Heat Transfer **115**, 7 (1993).

[10] D. Cahill, W. Ford, K. Goodson, G. Mahan, A. Majumdar, H. Maris, R. Merlin, and S. Phillpot, J. Appl. Phys. **93**, 793 (2003).

[11] J. Rupp and R. Birringer, Phys. Rev. B **36**, 7888 (1987).

[12] C. Dames, Annu. Rev. Heat Transf. **16**, 7 (2013).

[13] D. Zhao, X. Qian, X. Gu, S. Jajja, and R. Yang, J. Electron. Packag. **138**, (2016).

[14] D. Cahill, Rev. Sci. Instrum. **61**, 802 (1990).

[15] D. Cahill, Rev. Sci. Instrum. **75**, 5119 (2004).

[16] A. Jacquot, G. Chen, H. Scherrer, A. Dauscher, and B. Lenoir, Sensors Actuators A Phys. **117**, 203 (2005).

[17] A. Schmidt, R. Cheaito, and M. Chiesa, J. Appl. Phys. **107**, 024908 (2010).

[18] D. Zhao, X. Qian, X. Gu, S. Jajja, and R. Yang, J Electron Packag **138,** 040802 (2016).

[19] L. Qiu, N. Zhu, Y. Feng, E. Michaelides, G. Żyła, D. Jing, X. Zhang, P. Norris, C. Markides, and O. Mahian, Phys. Rep. **843**, 1 (2020).

[20] O. Breitenstein, W. Warta, and M. Langenkamp, *Lock-in Thermography: Basics and Use for Evaluating Electronic Devices and Materials* (Springer, Berlin/Heidelberg, Germany, 2010).

[21] T. Ishizaki, H. Nagano, S. Tanaka, N. Sakatani, T. Nakamura, T. Okada, R. Fujita, A. Alasli, T. Morita, M. Kikuiri, K. Amano, E. Kagawa, H. Yurimoto, T. Noguchi, R. Okazaki, H. Yabuta, H. Naraoka, K. Sakamoto, S. Tachibana, S. ichiro Watanabe, and Y. Tsuda, Int. J. Thermophys. **44**,

51 (2023).

[22] P. Liu, A. Alasli, L. Wang, and H. Nagano, Appl Therm Eng **255**, 123929 (2024).

[23] A. Alasli, R. Fujita, and H. Nagano, Int. J. Thermophys. **43**, 176 (2022).

[24] A. Alasli, A. Miura, R. Iguchi, H. Nagano, and K. Uchida, Sci. Technol. Adv. Mater. Methods **1**, 162 (2021).

[25] A. Alasli, T. Hirai, H. Nagano, and K. Uchida, Appl. Phys. Lett. **121**, 154104 (2022).

[26] A. Miura, H. Sepehri-Amin, K. Masuda, H. Tsuchiura, Y. Miura, R. Iguchi, Y. Sakuraba, J. Shiomi, K. Hono, and K. Uchida, Appl. Phys. Lett. **115**, 222403 (2019).

[27] K. Uchida, S. Daimon, R. Iguchi, and E. Saitoh, Nature **558**, 95 (2018).

[28] T. Seki, R. Iguchi, K. Takanashi, and K. Uchida, Appl. Phys. Lett. **112**, 152403 (2018).

[29] S. Daimon, R. Iguchi, T. Hioki, E. Saitoh, and K. Uchida, Nat. Commun. **7**, 13754 (2016).

[30] K. Uchida, Proc. Jpn Acad. Ser. B **97**, 69 (2021).

[31] Y. Hirayama, R. Iguchi, X. Miao, K. Hono, and K. Uchida, Appl. Phys. Lett. **111,** 163901 (2017).

[32] T. Hirai, R. Iguchi, A. Miura, and K. Uchida, Adv. Funct. Mater. **32,** 2201116 (2022).

[33] R. Iguchi, D. Fukuda, J. Kano, T. Teranishi, and K. Uchida, Appl. Phys. Lett. **122,** 082903 (2023).

[34] A. Wolf, P. Pohl, and R. Brendel, J. Appl. Phys. **96**, 6306 (2004).

[35] A. Salazar, A. Sánchez-Lavega, and J. Terrón, J. Appl. Phys. **84**, 3031 (1998).

[36] H. Carslaw and J. Jaeger, *Conduction of Heat in Solids*, Second eition (Clarendon press, Oxford, 1992).

[37] Y. Gu, X. Tang, Y. Xu, and I. Hatta, Jpn. J. Appl. Phys. **32**, L1365 (1993).

[38] C. Zhang, M. Giroux, T. Nour, and R. St-Gelais, Phys. Rev. Appl. **14**, 024072 (2020).

[39] M. Alam, M. Manoharan, M. Haque, C. Muratore, and A. Voevodin, J. Micromechanics Microengineering **22**, 045001 (2012).

[40] X. Zhang and C. Grigoropoulos, Rev. Sci. Instrum. **66**, 1115 (1995).

[41] J. Thornton, J. Vac. Sci. Technol. **11**, 666 (1974).

[42] G. Langer, J. Hartmann, and M. Reichling, Rev. Sci. Instrum. **68**, 1510 (1997).

[43] A. Lopeandía, F. Pi, and J. Rodríguez-Viejo, Appl. Phys. Lett. **92**, 122503 (2008).

[44] J. Yu, Z. Tang, F. Zhang, H. Ding, and Z. Huang, J. Heat Transfer **132**, 012403 (2010).

[45] J. Bourgoin, G. Allogho, and A. Haché, J. Appl. Phys. **108**, 073520 (2010).

[46] G. Langer, J. Hartmann, and M. Reichling, Rev. Sci. Instrum. **68**, 1510 (1997).

[47] P. Nath and K. Chopra, Thin Solid Films **20**, 53 (1974).

[48] L. Ouarbya, A. Tosser, and C. Tellier, J. Mater. Sci. **16**, 2287 (1981).

[49] J. Jin, J. Lee, and O. Kwon, Appl. Phys. Lett. **92**, 171910 (2008).

[50] A. Avery, S. Mason, D. Bassett, D. Wesenberg, and B. Zink, Phys. Rev. B **92**, 214410 (2015).

[51] Y. Zhu, X. Lang, W. Zheng, and Q. Jiang, ACS Nano **4**, 3781 (2010).

[52] G. White and S. Woods, Philos. Trans. R. Soc. London. Ser. A, Math. Phys. Sci. **251**, 273 (1959).

[53] J. Kimling, J. Gooth, and K. Nielsch, Phys. Rev. B **87**, 094409 (2013).

[54] J. Kimling, R. Wilson, K. Rott, J. Kimling, G. Reiss, and D. Cahill, Phys. Rev. B **91**, 144405 (2015).

[55] H. Nakayama, B. Xu, S. Iwamoto, K. Yamamoto, R. Iguchi, A. Miura, T. Hirai, Y. Miura, Y. Sakuraba, J. Shiomi, and K. Uchida, Appl. Phys. Lett. **118**, 042409 (2021).

[56] K. Uchida and R. Iguchi, J. Phys. Soc. Japan **90**, 122001 (2021).

[57] G. Wehmeyer, T. Yabuki, C. Monachon, J. Wu, and C. Dames, Appl. Phys. Rev. **4**, 041304 (2017).

Figures

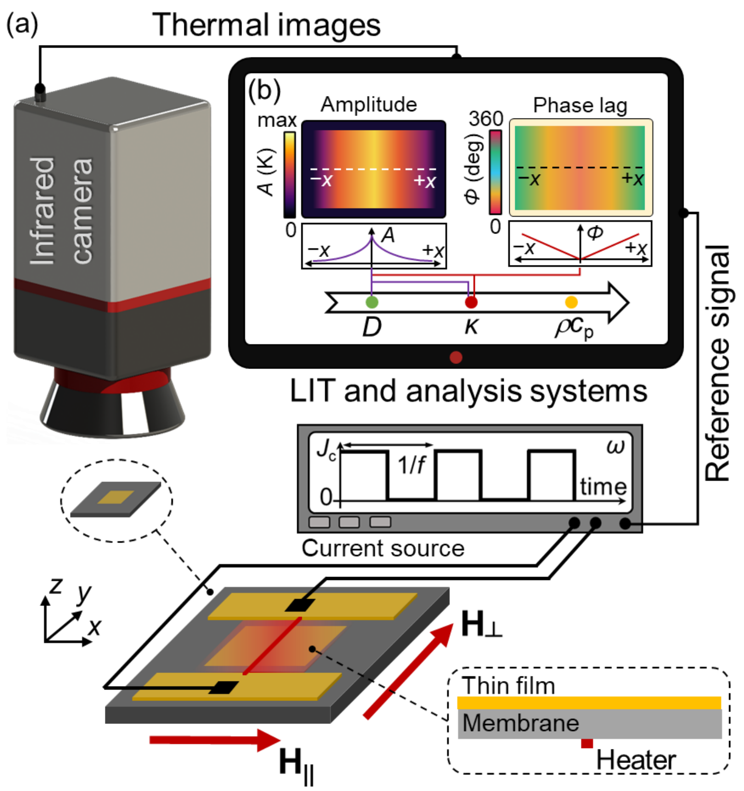

Fig. 1. (a) Schematic of the in-plane thermophysical properties measurement method based on the LIT technique. The sample can be a free-standing membrane or multilayered thin film deposited on the membrane. A thin metallic line heater is deposited on the other side of the membrane as a heating source. During measurements, the thin film is located to face the camera while the heater is excited by a square-wave charge current with the frequency f and amplitude J_c with DC offset $J_\mathrm{c}/2$. A and ϕ denote the lock-in amplitude and phase of the temperature modulation induced by the line heater, respectively. $\mathbf{H}_\parallel$ and $\mathbf{H}_\perp$ denote the in-plane external magnetic field applied along the parallel (x) and perpendicular (y) directions to the in-plane thermal gradient ∇T induced by the line heater, respectively. (b) Thermal analyses sequence of LIT images for obtaining the in-plane thermal diffusivity D, in-plane thermal conductivity κ, and volumetric heat capacity ρc_p.

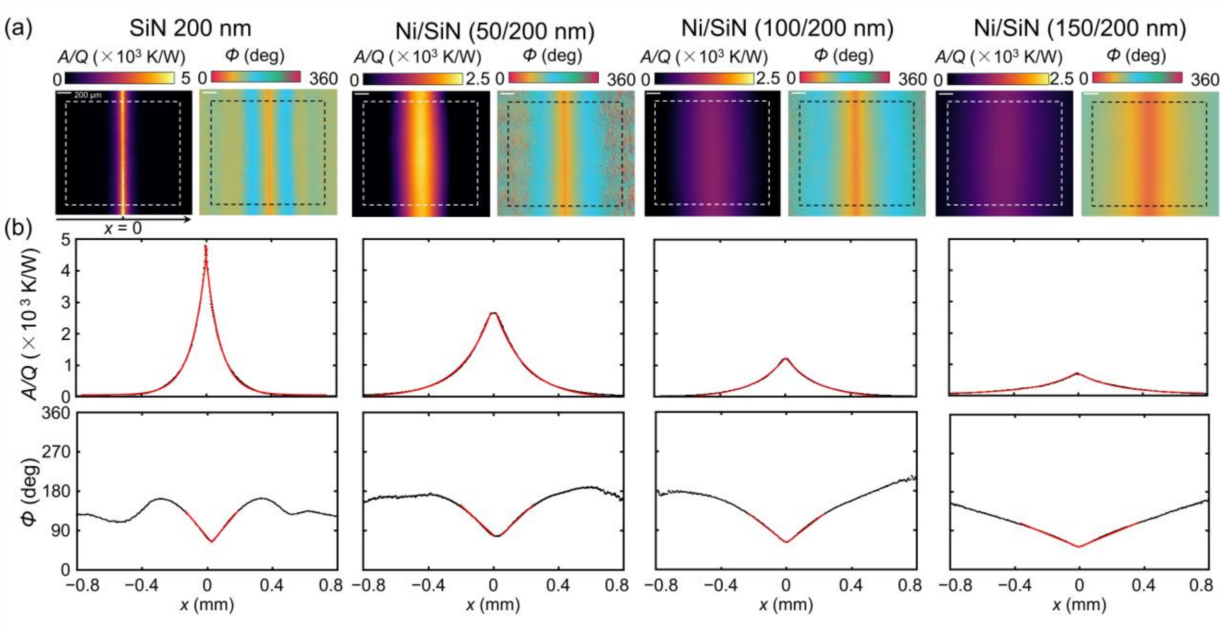

Fig. 2. (a) A/Q and ϕ images and (b) corresponding line profiles for the SiN membrane and Ni/SiN samples with different Ni thicknesses at *f* = 20 Hz. The line profiles were obtained by taking the average of the raw profiles over the center areas (dashed rectangles) of the samples. $x = 0$ in the line profiles was determined by the position of the line heater. The solid red lines in (b) represent the fitting results using Eqs. (4) and (5). The shown data in this figure were measured without applying an external magnetic field.

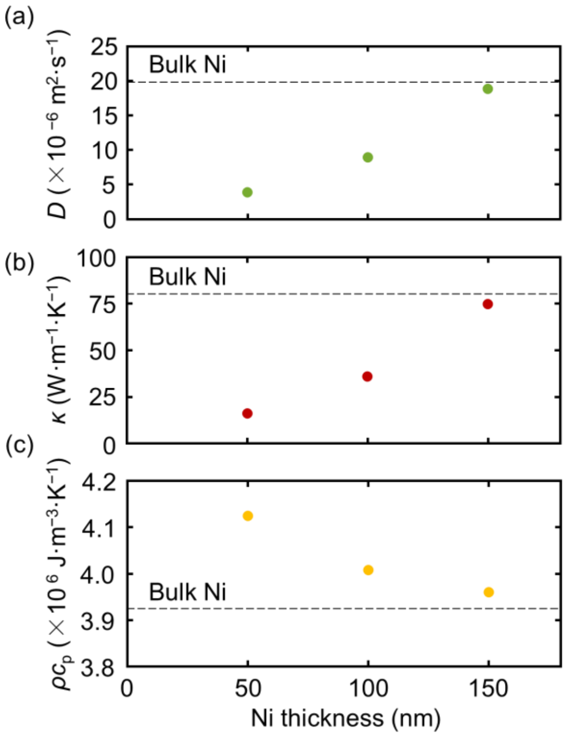

Fig. 3. Ni thickness dependence of (a) in-plane D, (b) in-plane κ, and (c) ρc_{p} at $T = 298$ K for the Ni thin films. D was obtained from the geometric mean $\sqrt{\Lambda_A \Lambda_\phi}$ with the thermal diffusion length Λ_A obtained from the A image and Λ_ϕ estimated from the ϕ image by fitting. κ was obtained with the combined heat transfer coefficient h from the difference $\frac{1}{\Lambda_A^2} - \frac{1}{\Lambda_\phi^2}$ and A at the line heater (x = 0) by fitting with the knowledge of D. ρc_{p} was then derived from D/κ. The dashed lines represent the values for bulk Ni.[24]

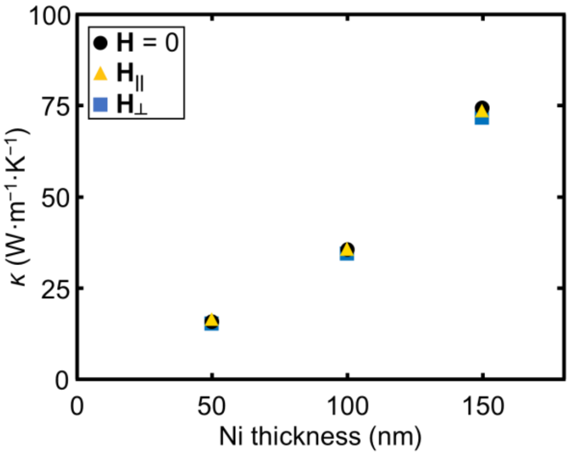

Fig. 4. Ni thickness dependence of in-plane κ at $T = 298$ K for different magnetic field configurations.